Unsupported Nickel Catalysts for Methane Catalytic Decomposition into Pure Hydrogen

Lu Zhou
State Key Laboratory of Materials-Oriented Chemical Engineering, College of Chemistry and Chemical Engineering, Nanjing Tech University, 5, Xinmofan Road, NanJing, JiangSu 210009, PR China

Yu Guo
State Key Laboratory of Materials-Oriented Chemical Engineering, College of Chemistry and Chemical Engineering, Nanjing Tech University, 5, Xinmofan Road, NanJing, JiangSu 210009, PR China

Kameyam Hideo
Dept. of Chemical Engineering, Tokyo University of Agriculture and Technology, 24-16, Nakacho 2, Koganei-shi, Tokyo 184-8588, Japan

DOI 10.1002/aic.14487
Published online May 13, 2014 in Wiley Online Library (wileyonlinelibrary.com)

Catalytic decomposition of methane to pure hydrogen is a reaction of crucial importance for clean energy, if the problem of catalyst separation is solved and the carbon material has an increased commercial value. Unsupported nickel catalysts were synthesized by fusion method. The catalyst derived from nickel nitrate forms heterogeneous octahedral NiO, whereas the nickel hydroxide precursor results in catalyst containing sponge-like NiO with folding lamellar structure of high porosity. The catalysts reactivity test was conducted with a fixed bed system at 1073 K. The catalyst subjected to hydrogen prereduction proved to be inactive. However, the methane prereduction was found to produce some coke to disperse the Ni particles and thus activated the catalyst. It was found that the higher concentration of methane resulted in a better methane conversion, but a higher deactivation rate. Carbon growth models were formulated to explain the formation of different types of carbon over Ni catalyst. © 2014 American Institute of Chemical Engineers *AIChE J*, 60: 2907–2917, 2014

Keywords: methane decomposition, unsupported catalyst, nickel catalyst, hydrogen production, carbon nanomaterial

Introduction

Methane catalytic decomposition (MCD) has been widely studied as an alternative way of methane steam reforming (MSR) to produce hydrogen, because MCD reaction

$$CH_4 \rightarrow C + 2H_2 \quad \Delta H_{298^\circ} = 74.8\,\text{kJ/mol} \tag{1}$$

does not produce CO or CO_2 as by-products, the need for water-gas shift and CO_2-removal stages, as required in conventional MSR, is eliminated.[1–3] Further, except the pure hydrogen produced from this process, the coproduced carbon nanomaterials (CNMs) have also been investigated extensively because of their excellent properties and great potentials for many utilization purposes.[4–6]

Because the main products of MCD are solid carbon and hydrogen gas, when conducting this process over a packed-bed reactor (PBR), the pressure drop will increase due to catalysts particle-size increment by the carbon deposition over the external surface of the catalyst particles. Meanwhile, the particle shape and density will also be altered. For experiments conducted over a long duration, a PBR will be gradually filled with solid carbon, eventually blocking reactant gas flow. Therefore, the selection of a catalytic reactor suitable for the MCD with continuous withdraw of the product carbon from the reactor is a very important aspect of the process development. Muradov[7,8] studied different types of reactors like tubular reactor, fluid wall reactor, free-volume reactor, PBR, fluidized-bed reactor (FBR), and spouted-bed reactor. He concluded that the FBR was the most promising reactor for large-scale operation as it provides a constant flow of solids through the reaction zone, making it suitable for continuous addition and withdrawal of catalyst particles from the reactor (similar to fluid catalytic cracking process). In a FBR, the bed of fine catalyst particles behaves like a well-mixed body of liquid giving rise to high particle-to-gas heat and mass-transfer rates.

In literatures, supported Ni catalyst has attracted much attention, due to its high reactivity and low price. Guevara et al.[9] reported a Ce-MCM-41 supported 50% Ni catalyst with 1400 min MCD reactivity of 70% CH_4 conversion at 853 K, 1 atm, $F/W = 1500$ mL/min g_{cat}. Otsuka et al.[10] developed a homemade carbon fiber supported 40% Ni

Additional Supporting Information may be found in the online version of this article.

Correspondence concerning this article should be addressed to Y. Guo at mguoyu@gmail.com.

catalysts with 1200 min MCD life of 10% CH_4 conversion at 803 K, 1 atm, $F/W = 1667$ mL/min·g_{cat}. Unfortunately, as to our knowledge, it should be noted that all the catalysts in literature show low MCD conversion and short life time. Although these issue could be overcome using the FBR reactor to get continuous stable hydrogen product, regeneration process is usually preferred over these supported catalysts system to make the process be more economical. The regeneration of deactivated catalysts is always done by a burning off or gasification process[11] which leads to CO_2 production in amounts nearly comparable to the quantity of CO_2 emitted by the MSR process.[12] Further, the regeneration process might result in the contamination of hydrogen with CO_2, which would require an additional purification step.[11] Conversely, it should be noted that the formation of traceable CO was observed which resulted from the unavoidable reaction of the carbonaceous residues with the oxygen in the support.[10,13] After the CO production rates stabilized, Choudhary et al.[14] reported 50 ppm CO in pure hydrogen of the MCD reaction over the 10% Ni/SiO_2 catalyst at 823 K, 1 atm, $F/W = 250$ mL/min·g_{cat}. From these standpoints, it is better to apply unsupported Ni catalyst for MCD. The bulk Ni catalyst, for instance, can be practically and easily removed off the carbon by-products by leaching with a mild acidic solution[15] or simply using a magnetic field,[16] but the separation of the Al_2O_3 or SiO_2 support may be quite burdensome.[10,13] This thus provides an easy recovery of the catalyst and a convenient way for the purification of the CNMs, which would make the process more economically attractive even without the aforementioned regeneration process. Furthermore, the unsupported Ni catalyst may prevent the formation of traceable CO.

Few literatures have focused on the MCD over unsupported Ni catalyst. Toebes et al.[17] found no MCD reactivity at 823 K on a Ni catalyst composed of 50–1000 nm polycrystalline Ni particles. Ermakova et al.[18] reported that by the addition of 10% Al_2O_3 or SiO_2 into pure Ni catalyst caused a decrease of nickel particle size from 65 to 11 nm; thus, they obtained a 10-fold increase of MCD reactivity. It is known that the support is to stabilize the easily aggregated metal particles. For this reason, less report is focused on using pure Ni catalyst for MCD process. In recent year, Wang and Lua[19] prepared unsupported metallic nickel particles by the decomposition of nickel oxalate in methane atmosphere. These Ni catalysts were tested in MCD reaction under moderate temperature from 798 to 848 K and showed promising activity. Li et al.[20] prepared nickel oxide with controlled crystallite size and fibrous morphology through the precipitation of nickel oxide from nickel acetate with the mediation of ethylene glycol. After reduction at different temperatures, the fibrous nickel oxide was converted to fibrous metallic nickel and showed good catalytic activity with carbon yields of 354−398 g C/g Ni at 773 K.

The thermodynamic equilibrium value was calculated using HSC Chemistry software in this study. It is obvious from those data that higher temperature and lower pressure favors this reaction. At temperature above 1073 K and pressure equal to 1 atm, very little methane remains in the gas phase and the hydrogen content overpasses 90%. So far, few studies have focused on the catalytic activity of pure metallic nickel catalysts under high temperature as 1073 K due to their insufficient thermal stability without the support under such severe catalytic reaction conditions.

In the present work, the MCD over a pure Ni catalyst was thoroughly studied at high temperature as 1073 K. Ni catalysts with varying particle sizes were prepared by simply fusing different nickel precursors. An Al_2O_3-supported Ni catalyst was also prepared as a comparison sample. The influence of prereduction method, CH_4 gas concentration on the catalyst reactivity and lifetime was studied using a fixed-bed system. The Ni particle size was screened by x-ray powder diffraction (XRD) and electron microscopy. A growth model of CNMs is formulated to interpret the influence of Ni particle size and the support over the carbon by-products morphologies.

Experimental

Preparation of Ni catalysts

Pure Ni catalyst was prepared using the fusion method.[21] The fusion catalyst is prepared by directly calcining powder of nickel precursors at 623 K for 3 h. Two kinds of fusion Ni catalysts were synthesized by fusing $Ni(NO_3)_2{\cdot}6H_2O$ and $Ni(OH)_2$, while they were designed as Ni-1 for nickel nitrate precursor and Ni-2 for nickel hydroxide precursor.

For comparison, an alumina-supported Ni catalyst was prepared by incipient impregnation with $Ni(NO_3)_2{\cdot}6H_2O$ solution. AEROXIDE® Alu 130 Al_2O_3 with 130 m^2/g Brunauer–Emmett–Teller (BET) surface area was used as the support. The Ni loading was controlled at 16 wt %. After impregnation, the Ni-supported sample was dried at 383 K for overnight and then calcined at 973 K for 5 h. The obtained catalyst was designed as Ni-3.

Characterization

The elemental composition of the samples was determined by the Atomic Emission Spectrometry-Inductively Coupled Plasma (AES-ICP) in a Thermo-Electron model 3580 instrument with a H_2SO_4/HNO_3 solution at 523 K.

The N_2 adsorption/desorption isotherms were performed using a Micromeritics ASAP2420. The samples were degassed for 2 h at 573 K before nitrogen adsorption. Surface areas of the samples were analyzed by multipoint BET analysis method, and pore volumes were estimated at $P/P_0 = 0.99$.

Temperature-programmed reduction (TPR) was performed on an Altamira Instrument. The catalyst powder (50 mg) was placed in a U-shaped quartz reactor and pretreated in flowing Ar (50 mL/min) for 0.5 h at 573 K, followed by cooling to room temperature under flowing Ar. The temperature was then raised from room temperature to 1273 K at a rate of 10 K/min under a 5% H_2/Ar flow (50 mL/min) atmosphere.

The XRD was recorded on a Bruker D8 Advanced A25 diffractometer in Bragg–Brentano geometry fitted with a copper tube operating at 40 kV and 40 mA. The catalyst powder was pressed into flakes and mounted in the chamber. The mean crystallite size was calculated from the Scherrer equation, where the particle shape factor was taken as 0.9.[22]

Scanning electron microscope (SEM) images were taken by the 600 FEG environmental scanning electron microscope. Transmission electron microscope (TEM) images were taken by a Titan G2 80–300 kV TEM from FEI Company (FEI Company, Hillsboro, OR) equipped with a 4 k × 4 k changed couple device camera model US4000 and an energy filter model GIF Tridiem from Gatan (Gatan, Pleasanton, CA). The specimens were prepared by ultrasonically suspending the sample

in ethanol. A drop of the suspension was then applied onto clean holy copper girds and dried in air.

Raman spectra of carbons deposited on the catalysts by the MCD reaction was measured with a laser Raman spectrometer (DXR Smart Raman Spectrometer). The spectra were taken with 514.5-nm line of an argon laser at room temperature. The incident laser power was adjusted to 2 mW at the sample. The spectra were recorded with a resolution of 4 cm^{-1}.

Catalytic reaction

The catalytic reaction was conducted in a PID Eng&Tech microactivity reactor equipped with a long stainless tube reactor (ID 9 mm, length 305 mm) which was heated by an electrical furnace under atmosphere pressure. Fifty milligram catalyst in size between 250 and 300 μm was loaded into the reactor, while the reaction temperature was controlled by a thermocouple placed into the middle of the catalyst layer. The CH_4 was diluted with N_2 using different ratios as 100% CH_4, 85% CH_4/N_2, or 20% CH_4/N_2, while the total gas flow rate was fixed at the same value of 37.5 mL/min in order to get a gas hourly space velocity at 45,000 mL/h·g_{cat}. Two reaction modes were adopted here. For Mode 1, after loading the catalyst, the reactor was heated to 773 K with 30 mL/min N_2, and then the flowing gas was switched to 30 mL/min H_2 to reduce the catalyst at 773 K for 1 h. After this prereduction, the gas was back to 30 mL/min N_2 to heat the catalyst to 1073 K. After this, the gas was changed to 37.5 mL/min reacting CH_4/N_2 to start the reaction. For Mode 2, the loaded catalyst was directly heated to 1073 K under 30 mL/min N_2, in the absence of hydrogen and then the gas was switched to 37.5 mL/min CH_4/N_2 mixture to begin the MCD reaction. The outlet gases were analyzed by an online GC (Varian 450-GC) and micro GC (Soprane MicroGC 3000).

Results and Discussion

Characterization of Ni-1, Ni-2, and Ni-3

Figure 1 shows the XRD patterns of the freshly prepared catalysts. As a control, AEROXIDE® (Alu 130 Al_2O_3) was also examined for blank support, which showed the typical peaks corresponding to gamma alumina. Only NiO peaks at $2\theta = 37°$, 44°, 62°, 75°, and 79°[23] were detected over Ni-1 and Ni-2. For the Ni-3 sample, besides the NiO reflections at

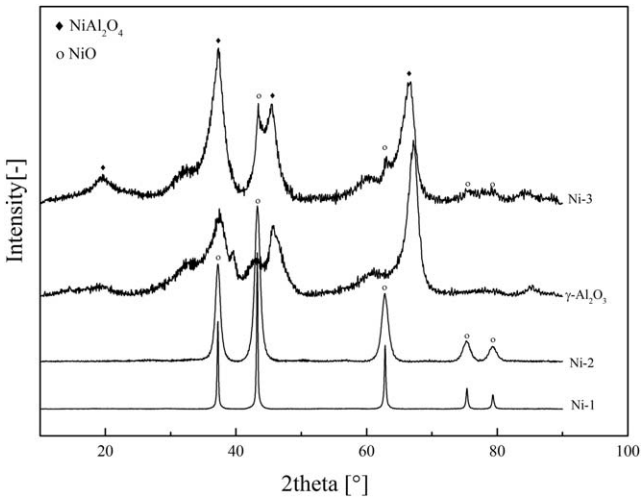

Figure 1. XRD patterns over fresh prepared samples.

$2\theta = 44°$, 62°, diffraction peaks at $2\theta = 19°$, 37°, and 66° were related to the nickel aluminate as $NiAl_2O_4$.[23]

The existence of different nickel oxide of Ni-1, Ni-2, and Ni-3 was also demonstrated by TPR profiles as shown in Figure 2. The reduction peaks of unsupported Ni-1 and Ni-2 samples were lower than 823 K, which was in agreement with Ni on both samples was in a bulk NiO state. Lua and Wang[24] reported a broad TPR reduction peak of pure NiO at 663–723 K. Robertson et al.[25] also reported TPR peak at 500–800 K representing the characteristic reduction of stoichiometric nickel oxide. On the Ni-Al TPR profile, four peaks were detected at 662, 756, 889, and 1053 K. The peaks at 662 and 756 K were ascribed to the reduction of bulk or free NiO on the alumina support. According to Roh et al.[26] and Zhou et al.,[27] the peak at 889 K can be assigned to the reduction of highly dispersed NiO, in a strong interaction with the alumina support. These NiO species were explained as fixed NiO and described in a form of NiO-Al_2O_3 or NiOx.[26,27] The peak at 1053 K was the reduction of surface nickel aluminate $NiAl_2O_4$, which was formed during high temperature as 973 K calcination of alumina-supported nickel catalyst.[27] For MCD reaction, Ni must be in a metallic state and thus a prereduction of the catalyst is required. From the TPR results, it is obvious that using an

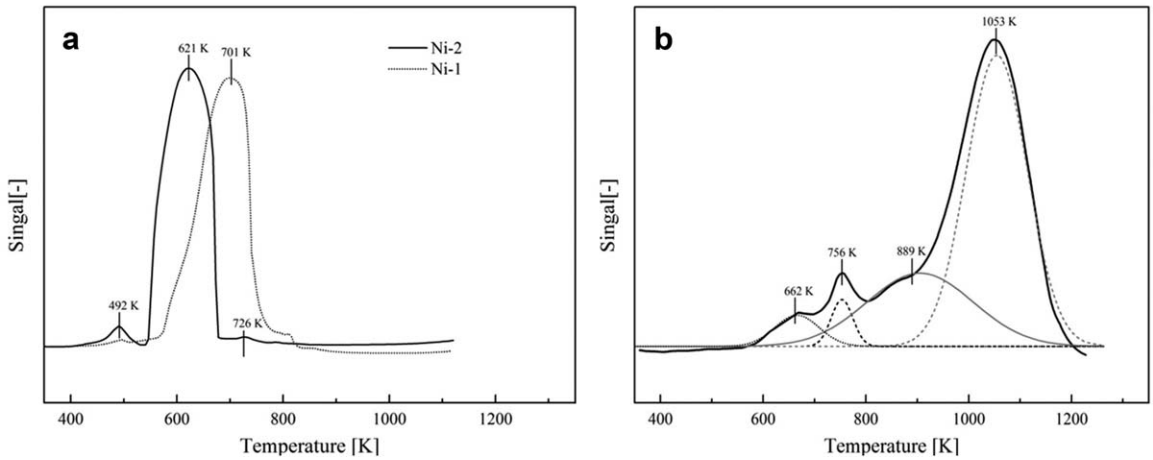

Figure 2. TPR profiles over different catalysts: (a) Ni-1 and Ni-2 catalysts; (b) Ni-3 catalyst.

Table 1. The Characterization of Prepared Catalysts

Samples	Ni Loading (wt %)	Surface Area (m^2/g)	Pore Volume (cc/g)	Nickel Species (%)			Mean Crystallite Size (nm)	
				NiO	NiO*x*	$NiAl_2O_4$	NiO[a]	NiO[b]
Ni-1	–	19.81	0.043	100	0	0	36	30
Ni-2	–	104.11	0.264	100	0	0	9	9
Ni-3	16.0	85.56	0.168	8	29	63	7	6
Alu 130	–	133.56	0.365	–	–	–	–	–

[a]XRD calculated size using Sherrer equation. It should be note the value is a geometric average.
[b]TEM image statistical analyzed size.
Not measured.

unsupported catalyst, a much lower reduction temperature as 700 K is sufficient; whereas for a supported catalyst a higher temperature as 1000 K is at least essential.

Based on the TPR curves area,[27] the quantitate calculation of different nickel species in three types as NiO, NiO*x*, and $NiAl_2O_4$ over the fresh catalysts was shown in Table 1. For supported Ni-3 catalyst, nickel oxides species ranged from 63% $NiAl_2O_4$, to 29% NiO*x* and to 8% NiO. For both unsupported Ni-1 and Ni-2 catalysts, the nickel existed in only pure NiO. However, it could be seen that the Ni-2 showed lower reduction temperature than that of Ni-1. Ji et al.[28] reported that the initial reduction temperature would be lower for bulk NiO with smaller particle size. Thus, the lower reduction temperature of Ni-2 might be attributed to the smaller size as shown in Table 1 (9 nm for Ni-2 in comparison with 36 nm for Ni-1). Further, the Ni-2 showed almost five times higher surface area and pore volume than those of Ni-1 in Table 1. These were explained by the different morphologies of NiO aggregates over Ni-1 and Ni-2 in Figure 3. The fused Ni-1 catalyst from nickel nitrate precursor formed heterogeneous octahedral NiO with wide size distribution. The Ni-2 from the nickel hydroxide resulted in sponge-like NiO with folding lamellar structure and high porosity but also with a wide size distribution. The different morphologies of NiO over Ni-1 and Ni-2 accounted for their differences in surface area and pore volume. The wider size distribution of NiO was corresponding to the broad TPR curves; as it has been previously reported, broad TPR peaks happened when reducing metal oxides with a wide size distribution.[29] Further, a trimodal pore-size distribution was observed over Ni-2 sample. The pores below 10 nm are believed to correspond to the pores described in Figure 3, and the larger pores are tentatively attributed to the mesopore existing in the NiO aggregates. For Ni-1 sample, a single pore-size distribution is observed, which could be illustrated as the size of cavities between adjacent primary particles. On the other part, as a comparison, Ni-3 as supported catalyst was also investigated. The Ni-3 shows moderate BET surface area, pore volume (Table 1), and a homogeneous (7 nm) crystallite size on the alumina surface.

MCD reactivity over prepared Ni-1 catalysts

In this study, MCD performance was examined at 1073 K and atmospheric pressure. Ni-1 was selected as a model of unsupported catalysts to investigate its MCD reactivity under two different modes. The Mode 1 showed a common way to activate the catalyst by reducing the NiO to metallic Ni using H_2 at 773 K for some period. It can be seen from the XRD patterns in Figure 4 that only metallic Ni exists over reduced Ni-1 sample. The mean Ni crystallite size calculated from the XRD is 223 nm. The Mode 1 H_2-reduced Ni-1 was subjected to MCD in Figure 5, but negligible methane conversion is observed during 15 h. Figure 6A shows that the 1-h H_2 prereduction leads to a coalescence of Ni into much larger particles, these particles are inactive for the MCD. Conversely, for the Mode 2, the Ni-1 without prereduction exhibits an interesting MCD behavior, which is assumed to occur into four steps: (1) activation of the catalyst; (2) induction period; (3) steady state; (4) deactivation step.

During Step 1, a high initial methane conversion occurs, which likely results from the combination effect of NiO reduction by CH_4 ($NiO + CH_4 \rightarrow$ "Ni" + $CO_x + H_2O + C + H_2$) and CH_4 steam reforming with this formed H_2O. This is demonstrated by the mass spectrum result. Flowing CH_4 gas through fresh Ni-1 at 1073 K, the formation of H_2, CO, CO_2, and H_2O resulted from the CH_4 reduce NiO and CH_4 steam reforming reaction during the initial 2 min was evidenced by the mass spectrometer. After that time, no signal of CO*x* was detected. The H_2O signal disappeared after 10 min, which means the NiO was completely reduced into Ni by the H_2. The XRD also showed that after 30 min, the NiO was completely reduced to "Ni" (Figure 4). Formation of coke was also demonstrated by XRD. This coke was considered to play the role of a support to disperse the reduced Ni. As shown in Figure 6a, the coke in gray color seemed to cut the connection of neighbored Ni particle in black color and thus somehow dispersed the Ni particle. Over a 10% Ni/SiO_2 catalyst, Choudhary et al.[14] reported that the CO concentration is 0.2% initially, drops below 100 ppm in 90 min, and then remains at about 50 ppm for 6 h after, followed by a slight increase during the deactivation stage of the catalyst. This means that the CO formed during all the MCD process over a supported catalyst system. For the CH_4 reduction process of unsupported metal catalysts, like Ni-1 in this study, although it is unavoidable, there will be no contamination of CO*x* after all the oxygen in the catalyst is consumed in a rather short period. Therefore, considering the *in situ* catalysts reduction with CH_4 reactant gas instead of additional H_2 gas, the more dispersion of Ni and no CO*x* contamination after a short period, the CH_4 reduction may be a positive way to active the unsupported metal catalysts.

During the following Steps 2–4, the methane conversion was found to increase with time on stream until a relatively stable steady state is achieved and then a deactivation occurs gradually. We made the hypothesis that the Ni-1 structure was changed during this period. To evidence what happened during Steps 2–4, the MCD reaction was stopped at 0.5, 1.5, 2, 3, and 10 h, and the samples were subjected to XRD, SEM, and TEM analyses (Figure 5 Mode 2). From Figure 6,

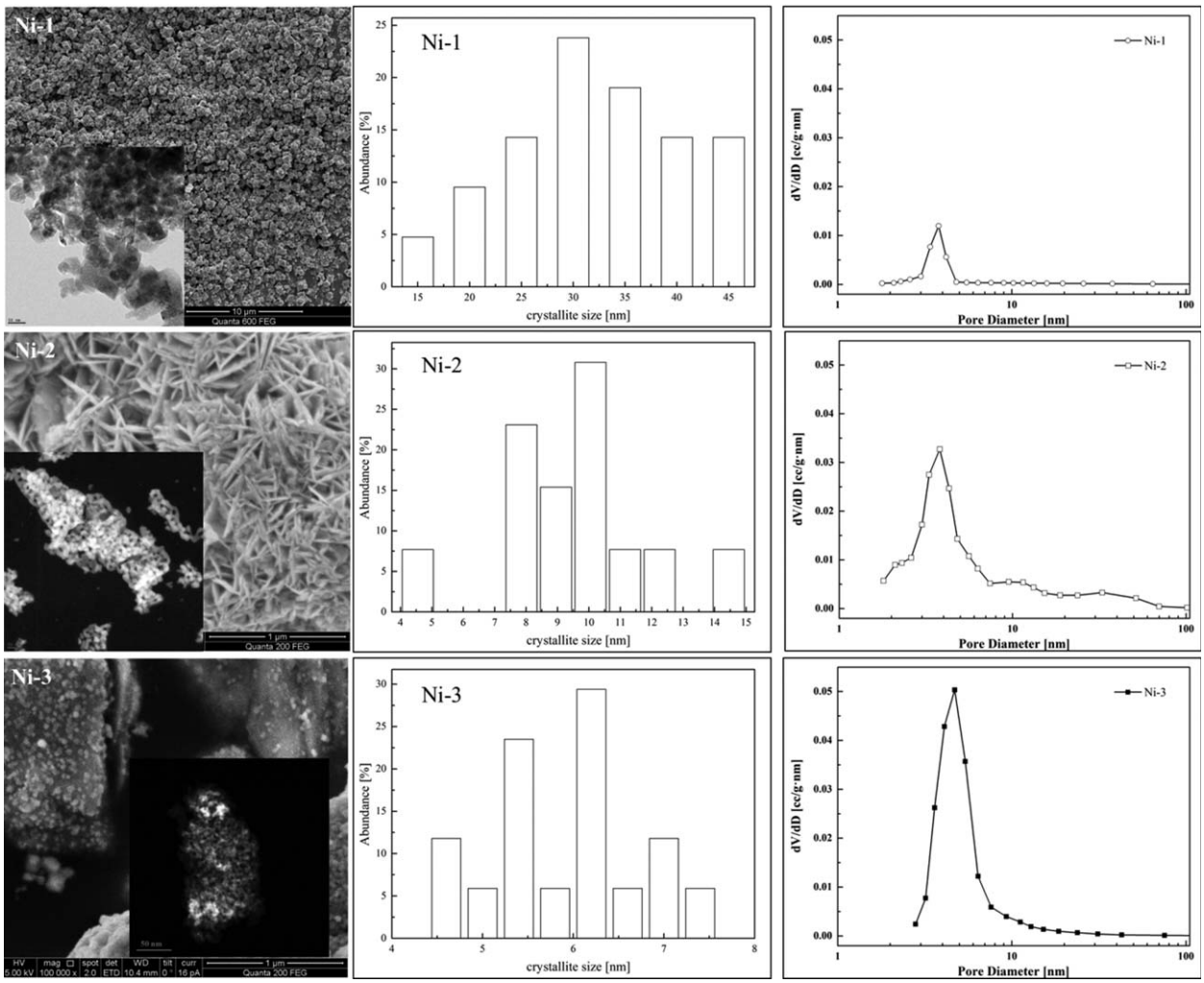

Figure 3. SEM, TEM images, crystallite and pore-size distribution over fresh prepared catalysts.

it could be found that the Ni on the Ni-1 became more and more dispersed with the increment of methane flowing period over the Ni-1 sample under Mode 2. The XRD analyses in Figure 7 showed the increment of coking amount over Ni-1, as the graphite peak became much more pronounced with time, while the Ni was still in metallic state. However, the size calculated from XRD showed that the crystallite size of Ni was becoming smaller with time, from 150 nm at initial 0.5 h to 106 nm at 3 h. This Ni size was somehow kept stable until the total deactivation of Ni-1 at 10 h occurred. However, it should be noted here that the size calculated from XRD is a geometric average of a possibly wider distribution. Several literatures reported that the nickel catalyst might be considered as self-organizing system during MCD reaction.[30] Nickel particles underwent active evolution to seek to some thermodynamically favorable size. Ermakova et al.[30] measured the size change during MCD at 823 K over a series of SiO_2 supported 10% Ni catalysts with varied nickel size from 15 to 60 nm. They found, after 2 h in MCD, all the Ni over these samples were sintered or fragmented to 31–35 nm. Thus, they concluded that the 31–35 nm Ni over SiO_2 was the optimal size for the MCD reaction. Therefore, it could be reasonable to conclude the 100-nm Ni might be a favorite size for the MCD reaction at 1073 K in this study over unsupported Ni catalyst system.

Figure 8 shows the influence of methane concentration on the MCD reactivity in Mode 2. The results indicates that an increase in the methane partial pressure leads to a high initial reaction rate in Mode 2, but to a shorter stable period in

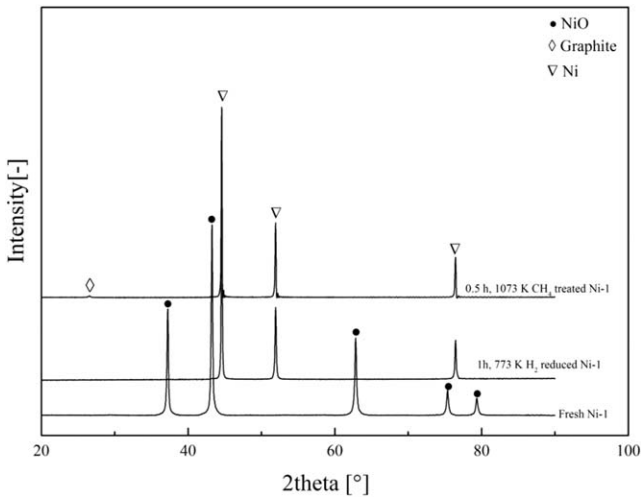

Figure 4. XRD patterns over activated Ni-1 samples with different routes.

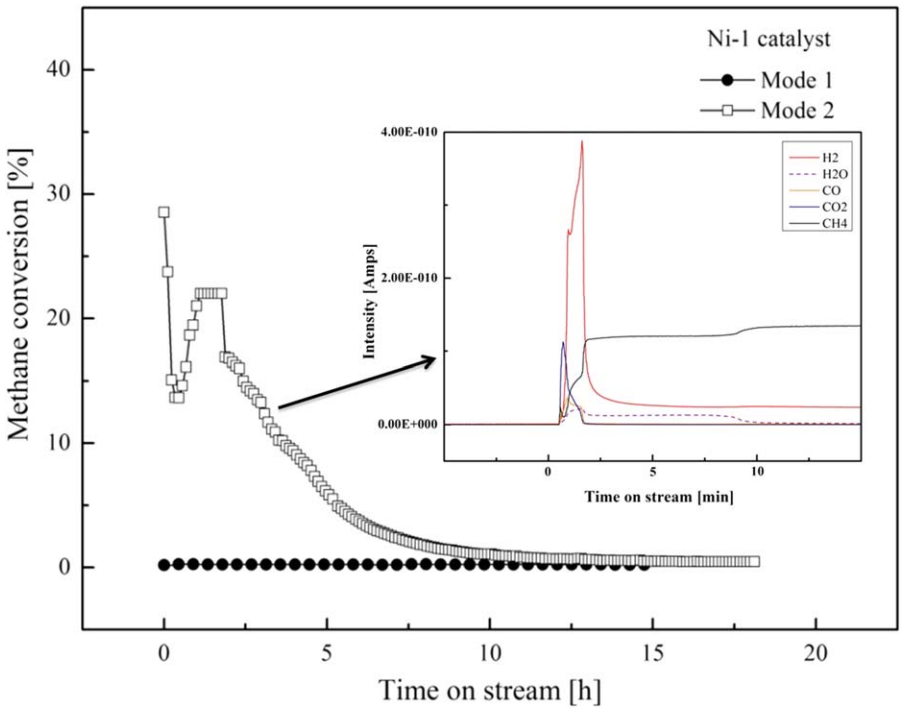

Figure 5. Influence of reaction route over Ni-1 catalyst MCD reactivity, CH_4 concentration 100%.

[Color figure can be viewed in the online issue, which is available at wileyonlinelibrary.com.]

Step 3 and a greater deactivation rate in Step 4. Under 100 and 85% CH_4, the Ni-1 catalyst become totally deactivated after 7 h in mode 2, while in 20% CH_4 a stable conversion (8%) is observed during 20 h. It is suggested that he higher concentration of methane boosted the diffusion-precipitation process through the nickel crystallite. This in turn would results in the higher methane conversion. But the reaction rate would definitely cause the greater formation of "carbon species" which could encapsulate and deactivate the nickel metallic crystallite.[31]

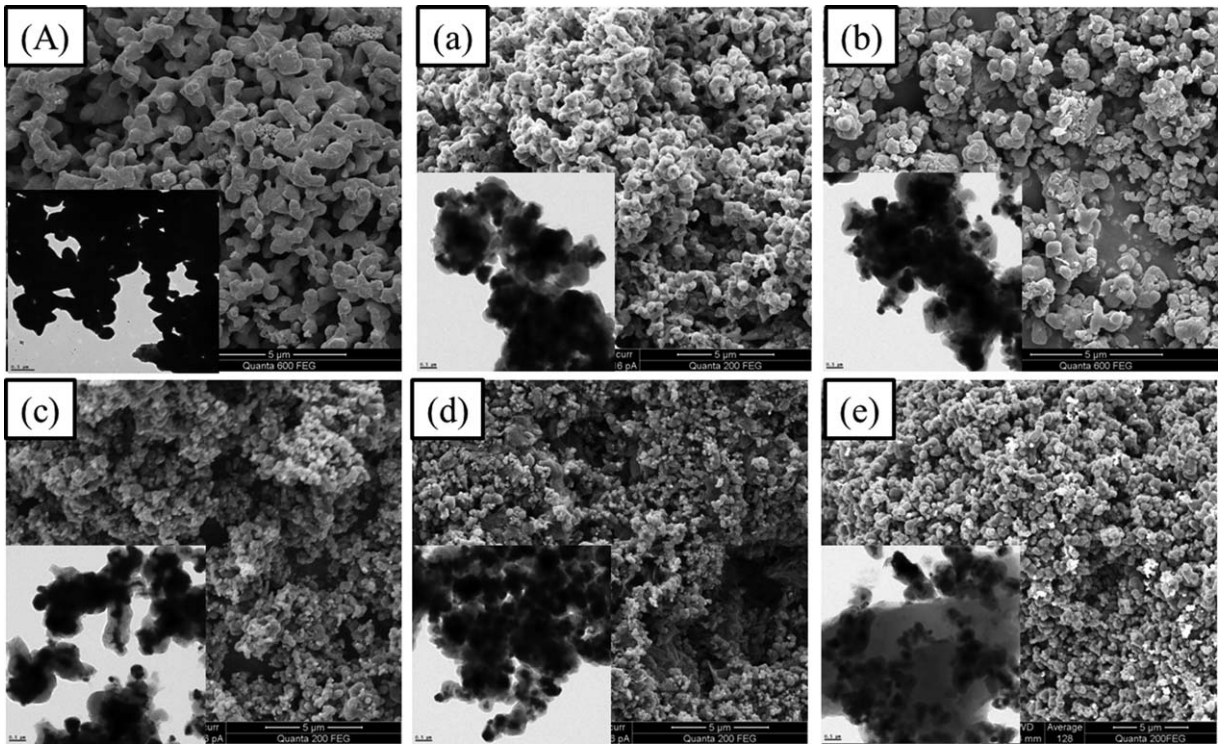

Figure 6. Morphologies of Ni-1 under different activation modes: Mode 1: (A) 1h; Mode 2: (a) 0.5 h; (b) 1.5 h; (c) 2 h; (d) 3 h; (e) 10 h.

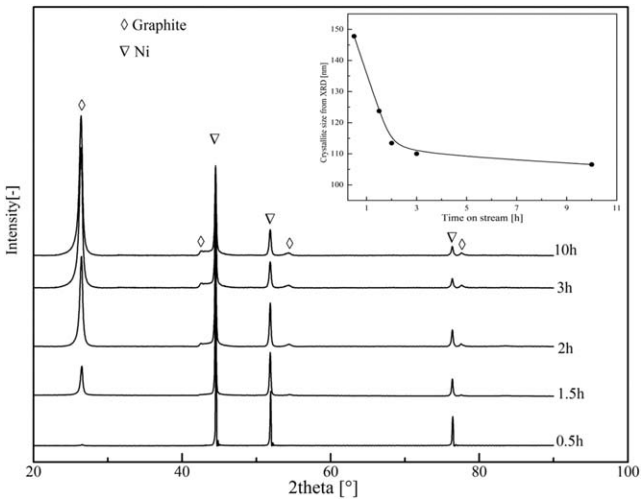

Figure 7. XRD patterns over Ni-1 in Figure 55 Mode 2 at different time.

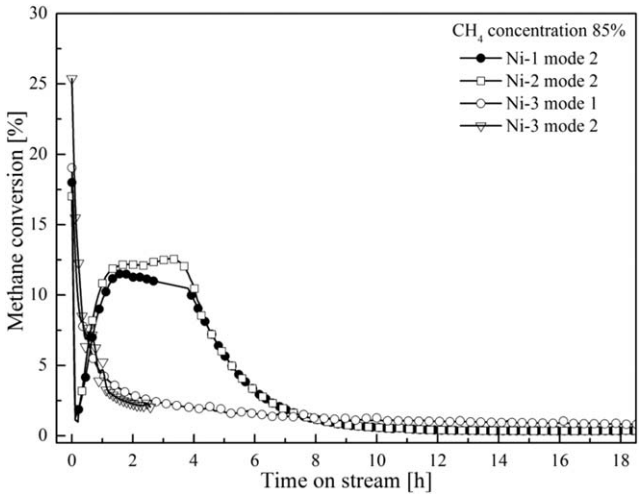

Figure 9. MCD reaction over Ni-2 and Ni-3 catalysts under different routes with 85% CH_4.

MCD reactivity over prepared Ni-2 and Ni-3 catalysts

The results of MCD over Ni-2 and Ni-3 catalysts under different modes are shown in Figure 9. The Ni-2 exhibits almost the same reactivity profile as the Ni-1 under Mode 2. The size calculated from spent Ni-2 XRD pattern (see Supporting Information) shows a 103-nm crystallite Ni over the deactivated Ni-2. Although the initial size of NiO over Ni-2 was much smaller than that of Ni-1, the deactivated Ni-2 catalyst nickel size was the same as that of Ni-1, and the value was just corresponding with our speculated optimal size for MCD reaction with unsupported nickel catalysts system. Conversely, over the supported Ni-3 catalyst, the influence of different modes over the MCD reactivity was negligible, both catalysts under Modes 1 and 2 exhibited similar performances. This might be considered as the support dispersed the Ni well enough as in Figure 3 to resist the sintering resulted from the H_2 prereduction. Although the Ni-3 presented high initial MCD reactivity, the catalyst became totally deactivated during 3 h. The XRD pattern over 1 h, 1073 K reduced Ni-3 showed the existence of Ni^0 peak and the disappearance of $NiAl_2O_4$, which illustrating 1073 K temperature was high enough to reduce the $NiAl_2O_4$ into Ni. This temperature was corresponding to the TPR result. The spent Ni-3 under Modes 1 and 2 XRD calculated the same Ni crystallite size of 18 nm, which was near the reduced fresh Ni-Al catalyst of 17 nm. This was different from the size change trend of unsupported Ni-1 and Ni-2 systems.

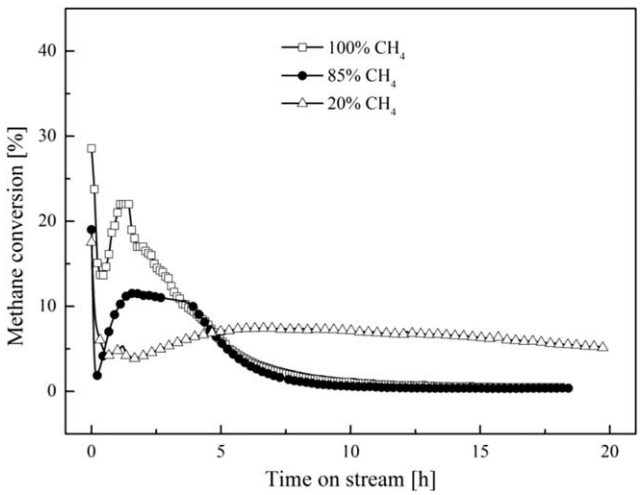

Figure 8. MCD reaction over Ni-1 catalyst under different CH_4 concentration in Mode 2.

Deposited carbon morphology and MCD reaction models over supported and unsupported Ni catalysts

Figure 10 shows the morphologies of deposited carbon over Ni-1, Ni-2, and Ni-3 samples using Mode 2. Over the Ni-1 catalyst, only carbon nano onions (CNOs) with quasi-spherical morphology are obtained. These CNOs have a diameter in the range of 30–60 nm, whereas the Ni encapsulated with the CNOs is about 70–100 nm. Figure 11 shows the Raman spectra of the CNOs over the deactivated Ni-1. The D band indicates the vibrations of carbon atoms with dangling bonds for in-plane terminations of disordered graphite. The G band represents the vibrations of all sp2 bonded carbon atoms in a two-dimensional hexagonal lattice.[32,33] The ratio of the area of D band to that of the G band (I_D/I_G) is considered an index for the crystalline order of graphite.[34] The lower I_D/I_G value represents higher graphitization of carbons. In our case, the I_D/I_G is 0.5, revealing that the CNOs over the Ni-1 had a high graphitic crystallinity, which is also demonstrated by the XRD in Figure 7. Over the Ni-2 catalyst, majority of the carbon existed in the CNOs form, while some multiple wall carbon nanotubes (MWCNTs) are also observed. The diameter of these MWCNTs varies between 46 and 70 nm. The Ni with the same size as that of the MWCNTs diameter is found located at the tip of the MWCNTs. For the supported Ni-3 catalyst, it could be seen that except a few CNOs over >70 nm Ni particles, most deposited carbons are MWCNTs. However, these MWCNTs are different from those observed over Ni-2, because the MWCNTS over Ni-3 sample have close end without Ni particle on the tip and/or embedded with small pieces of Ni inside their tubes.

Although some researchers[9] tried to illustrate carbon deposition mechanism over supported nickel catalyst, such mechanism of carbon growth over Ni particles over unsupported catalysts was never mentioned in literature. Based on the MCD results shown in Figure 9, Ni crystallite size changes

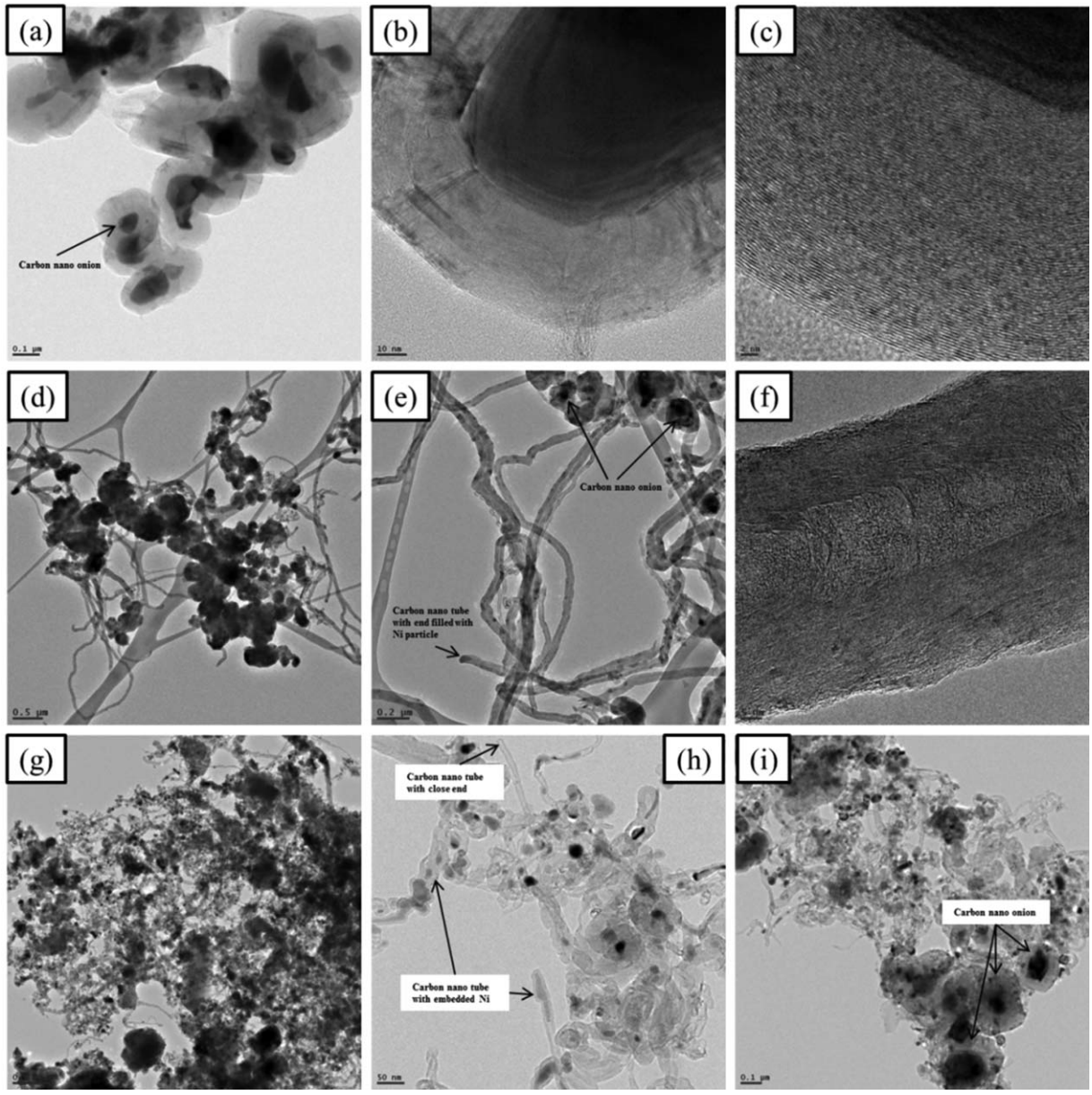

Figure 10. TEM micrographs of the carbon deposited on different catalysts: (a)–(c) Ni-1; (d)–(f) Ni-2; (g)–(i) Ni-3.

in Figure 7 and different carbon morphologies given in Figure 10, MCD reaction models for unsupported Ni-1, Ni-2 and supported Ni-3 catalysts are proposed in Figure 12.

Let us summarize the data here:

For unsupported Ni-1, after the 0.5 h methane prereduction (Figure 6a), Figure 7 shows the average Ni particle size is about 150 nm, but with wide size distribution during 70–200 nm in Figure 6b. However, after 18 h MCR reaction in Figure 9, we find only Ni particles of 70–100 nm, which is the size of the inside core of CNOs.

For unsupported Ni-2, after the 0.5 h methane prereduction, the average Ni particle size is about 50 nm with size distribution ranging between 30 and 100 nm. After 18 h MCR reaction, we find Ni particles of 70–100 nm, which fits with the internal core of CNOs, and some Ni particles of 30–70 nm on the tip of MWCNTs with an open end.

For supported Ni-3, after the 0.5 h methane prereduction, the average Ni size is about 20 nm with a relatively homogeneous size distribution, only few Ni particles are situated at 70 nm. After 18 h MCR reaction, we find Ni particles in 20 nm embedded in MWCNTs chain structure and some small pieces of Ni particles on the tip MWCNTs with a close end.

Three steps are to occur assumed during the MCD reaction: CH_4 activation-decomposition on the Ni particle to produce H_2 and carbon, carbon diffusion through the bulk of Ni particle and carbon precipitation. The coke morphology is very likely directly related to the balance between CH_4 activation-decomposition rate and its diffusion-graphite formation rate.[9]

By simply comparing the Ni-1, Ni-2, and Ni-3, we can conclude that the CNOs only formed over the Ni particle of 70–100 nm, whereas the MWCNTs formed on the Ni particle smaller than 70 nm. It is obvious that if the carbon deposition rate is higher than the carbon diffusion-graphite formation rate, the Ni will be encapsulated by the coke to form CNOs with the mechanism illustrated in Figure 12.

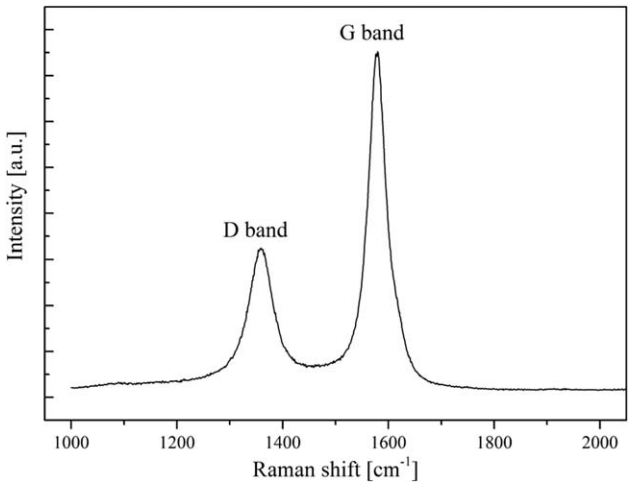

Figure 11. Raman spectra of the deactivated Ni-1.

Thus, this would suggest that the carbon deposition rate is higher than the graphite formation rate on the Ni of 70–100 nm.

But, it should be noticed here that even on the Ni bigger than 100 nm, CNOs with core of Ni smaller than 100 are shown on Ni-1 sample. This is explained here with a breakdown mechanism as follows perhaps the CH_4 activation-decomposition rate on the Ni bigger than 100 nm is much slower than the diffusion-graphite formation rate. This, thus, results in more deposited surface carbon on Ni (100) or Ni (110) planes dissolves into the nickel particles on the gas side,[30] and the carbon concentration gradient would create a driving force to diffuse the carbon through the bulk nickel particles until the carbon accumulate in the form of graphite layers on the Ni (111) plane.[31] The graphitic layer is initially oriented in parallel to the Ni particle crystallographic planes. At a certain moment, the nickel particle becomes fluid while its tail would extend due to some thermodynamic reason or the pressure from the outside graphite layers. The graphite layer would be distorted to encapsulate part of the nickel particle. With the time on stream, the continually growing up of the graphite layer would finally cut off the encapsulated nickel from the original bigger Ni particle. This process would split the initial big nickel particle into several Ni fragments until cut the original Ni with the thermodynamically favorable size at about 106 nm in this study. Over this size, CH_4 activation-decomposition would be rather higher than diffusion-graphite formation rate, resulting in the fast encapsulation of entire Ni particle with carbon to form CNOs and deactivate the catalyst completely.

For the growing up of MWCNT with Ni on its tip, the mechanism is explained by an equal CH_4 activation-decomposition rate with diffusion-graphite formation rate in this study. The continually carbon diffusion from Ni (100) or Ni (110) planes to Ni (111) plane would thermodynamically favor the growing up of carbon tube form rather than the carbon accumulation.[30] It is clear that for unsupported Ni catalyst Ni-2, we only observed MWCNTs with open on while Ni particle on the tip, while MWCNTs with close end of Ni particle on the bottom or embedded with small pieces of Ni inside their tubes are observed on Ni-3. These differences would be explained by the different metal-support interaction. For Ni-2, there is no support and thus the Ni particles smaller than 70 nm is of high mobility, especially under the high temperature 1073 K in this study. The growing up of the MWCNTs would support the Ni on the tip. Conversely, for supported Ni-3, the Ni reduced from the NiO, NiO*x*, and $NiAl_2O_4$ in Figure 2(b) was in a strong interaction with the support and thus the Ni was difficult to move. It is known the Ni from the $NiAl_2O_4$ shows the strongest metal-support interaction, followed by Ni from NiO*x* and Ni from NiO.[27] The strong metal-support interaction between Ni of $NiAl_2O_4$ and support might make the carbon precipitate on the other side of the exposed surface of the Ni particles, rather than the interface between the lower portion of Ni and support. This would make the carbon nanotube constructed in the surface of Ni particle toward gas–solid interface. As a result, the Ni particle would be fixed on the support, but leaving the carbon tube growing with a closed end of Ni on its bottom. The reduction of NiO*x* and NiO would result in Ni particles with weak metal-support interaction. Over these Ni particles, the MWCNTs with closed end form with the same mechanism. But with the growing of the nanotubes, their part in contact with the Ni particles became narrowed and the tail of the Ni particles might be pulled inside the carbon capsule, forming a small

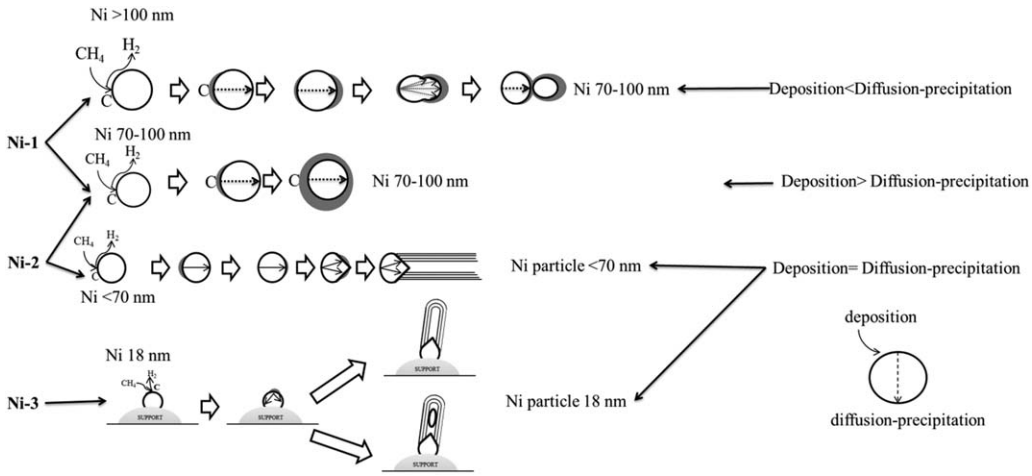

Figure 12. MCD reaction mechanism over different catalysts.

pieces of Ni particle encapsulated in the MWCNTs with diameter the same as the inner diameter of the carbon tube.

Conclusions

In this study, using a simple fusing method, two kinds of unsupported Ni catalysts Ni-1 and Ni-2 were prepared from different precursors. The influence of reaction routes, reactant gas concentration on the catalyst MCD reactivity, and lifetime was studied. A growth model of CNMs was also formulated to interpret the influence of Ni particle size and the support over the carbon by-products morphology. The following are the conclusions drawn from this work:

1. The fused Ni-1 catalyst from nickel nitrate precursor formed heterogeneous octahedral NiO, whereas the Ni-2 from the nickel hydroxide resulted in sponge-like NiO with folding lamellar structure with high porosity. Both catalysts showed a wide range of size distribution, as compared with the alumina supported Ni-Alu catalyst.

2. Hydrogen prereduction severely sintered the unsupported Ni catalysts and thus made the Ni-1 inactive for MCD. As an alternative way, the methane prereduction would produce some coke to act like a support to disperse Ni particles. The Ni-1 with methane prereduction showed better MCD reactivity at 1073 K.

3. The higher concentration of methane boosted the diffusion-precipitation process through the nickel crystallite. This in turn resulted in the higher methane conversion, but higher deactivation rate.

4. Carbon growth models were built to explain the different MCD reactivity and carbon morphologies over Ni-1, Ni-2, and Ni-3. Big size >70 nm Ni would form the CNOs. Ni size <70 nm had the same rate of diffusion-precipitation and carbon deposition, and thus tended to form nanotubes. For the pure Ni catalyst, nanotube would support the Ni particle on the tip of the MWCNTs. Over the supported Ni-3 catalyst, MWCNTs were also observed, but with different structures like MWCNTs embedding small pieces of Ni particles and MWCNTs with closed end without Ni particle on the tip, because of the metal-support interaction.

Literature Cited

1. Echegoyen Y, Suelves I, Lazaro MJ, Moliner R, Palacios JM. Hydrogen production by thermocatalytic decomposition of methane over Ni-Al and Ni-Cu-Al catalysts: effect of calcination temperature. *J Power Sources*. (2007);169:150–157.
2. Lijun J, Huanhuan S, Jianbo Z, Ping L, Zhiyuan H, Bo Q, Haoquan H. Preparation of activated carbon supported Fe–Al2O3 catalyst and its application for hydrogen production by catalytic methane decomposition. *Int J Hydrogen Energy*. (2013);38:10373–10380.
3. Gaowei W, Yi J, Guojuan L, Yongdan L. Production of hydrogen and nanocarbon from catalytic decomposition of methane over a Ni–Fe/Al2O3 catalyst. *Energy Fuels*. (2013);27:4448–4456.
4. Li Y, Chen J, Qin Y, Chang L. Simultaneous production of hydrogen and nanocarbon from decomposition of methane on a nickel-based catalyst. *Energy Fuels*. (2000);14:1188–1194.
5. Wang H, Baker RTK. Decomposition of methane over a Ni-Cu-MgO catalyst to produce hydrogen and carbon nanofibers. *J Phys Chem B*. (2004);108:20273–20277.
6. Ermakova MA, Ermakov DY, Kuvshinov GG. Effective catalysts for direct cracking of methane to produce hydrogen and filamentous carbon: part I. Nickel catalysts. *Appl Catal A: Gen*. (2000);201:61–70.
7. Muradov N. Thermocatalytic CO_2-free production of hydrogen from hydrocarbon fuels. Proceedings of the (2002) U.S. DOE Hydrogen Program Review, May 6-10, 2002, Golden, CO, NREL/CP-610-32405. 2002.
8. Muradov N. Thermocatalytic CO_2-free production of hydrogen from hydrocarbon fuels. Proceedings of the (2001) U.S. Department of Energy, Hydrogen Program Review, Baltimore, MD, April 17-19, 2001, NREL/CP-570-30535. 2001.
9. Guevara JC, Wang JA, Chen LF, Valenzuela MA, Salas P, García-Ruiz A, Toledo JA, Cortes-Jácome MA, Angeles-Chavez C, Novaro O. Ni/Ce-MCM-41 mesostructured catalysts for simultaneous production of hydrogen and nanocarbon via methane decomposition. *Int J Hydrogen Energy*. (2010);35:3509–3521.
10. Otsuka K, Ogihara H, Takenaka S. Decomposition of methane over Ni catalysts supported on carbon fibers formed from different hydrocarbons. *Carbon*. (2003);41:223–233.
11. Lee KK, Han GY, Yoon KJ, Lee BK. Thermocatalytic hydrogen production from the methane in a fluidized bed with activated carbon catalyst. *Catal Today*. (2004);93:81–86.
12. Muradov N, Chen Z, Smith F. Fossil hydrogen with reduced CO2 emission: modeling thermocatalytic decomposition of methane in a fluidized bed of carbon particles. *Int J Hydrogen Energy*. (2005);30:1149–1158.
13. Reshetenko TV, Avdeeva LB, Ismagilov ZR, Chuvilin AL, Fenelonov VB. Catalytic filamentous carbon-supported Ni for low-temperature methane decomposition. *Catal Today*. (2005);115:102–103.
14. Choudhary TV, Sivadinarayana C, Chusuei CC, Klinghoffer A, Goodman DW. Hydrogen production via catalytic decomposition of methane. *J Catal*. (2001);199:9–18.
15. Li Y, Li D, Wang G. Methane decomposition to COx-free hydrogen and nano-carbon material on group 8–10 base metal catalysts: a review. *Catal Today*. (2011);162:1–48.
16. Jana P, O'Shea VAD, Coronado JM, Serrano DP. Cobalt based catalysts prepared by Pechini method for CO2 free hydrogen production by methane decomposition. *Int J Hydrogen Energy*. (2010);35:10285–10294.
17. Toebes ML, Bitter JH, Dillen AJV, Jong KPD. Impact of the structure and reactivity of nickel particles on the catalytic growth of carbon nanofibers. *Catal Today*. (2002);76:33–42.
18. Ermakova MA, Ermakov DY, Kuvshinov GC, Plyasova LM. New nickel catalysts for the formation of filamentous carbon in the reaction of methane decomposition. *J Catal*. (1999);187:77–84.
19. Wang HY, Lua AC. Development of metallic nickel nanoparticle catalyst for the decomposition of methane into hydrogen and carbon nanofibers. *J Phys Chem C*. (2012);116:26765–26775.
20. Li Y, Zhang B, Xie X, Liu J, Xu Y, Shen W. Novel Ni catalysts for methane decomposition to hydrogen and carbon nanofibers. *J Catal*. (2006);238:412–424.
21. Suelves I, Lázaro MJ, Moliner R, Corbella BM, Palacios JM. Hydrogen production by thermo catalytic decomposition of methane on Ni-Based catalysts: influence of operation conditions on catalyst deactivation and carbon characteristics. *Int J Hydrogen Energy*. (2005);30:1555–1567.
22. Cullity BD. *Elements of X-ray Diffraction*, 2nd ed. Menlo Park, CA: Addison–Wesley, (1978).
23. Han YS, Li JB, Ning XS, Yang XZ, Chi B. Study on NiO excess in preparing $NiAl_2O_4$. *Mater Sci Eng A*. (2004);369:241–244.
24. Lua AC, Wang HY. Decomposition of methane over unsupported porous nickel and alloy catalyst. *Appl Catal B*. (2013);132–133:469–478.
25. Robertson SD, Mcnicol BD, Bass JH, Kloet SC, Jenkins JW. Determination of reducibility and identification of alloying in copper-nickel-on-silica catalysts by temperature-programmed reduction. *J Catal*. (1975);37:424–431.
26. Roh HS, Jun KW, Park SE. Methane-reforming reactions over Ni/Ce-ZrO2/α-Al2O3 catalysts. *Appl Catal A*. (2003);251:275–283.
27. Zhou L, Guo Y, Sakurai M, Kameyama H. Study of porous anodic alumina supported plate-type catalysts during daily start-up and shutdown operation of methane steam reforming. *Appl Catal A*. (2009);364:101–107.
28. Ji YG, Zhao Z, Duan AJ, Jiang GY, Liu J. Comparative study on the formation and reduction of bulk and Al_2O_3-supported cobalt oxides by H2-TPR technique. *J Phys Chem C*. (2009);113:7186–7199.
29. Villaverde MM, Bertero NM, Garetto TF, Marchi AJ. Selective liquid-phase hydrogenation of furfural to furfuryl alcohol over Cu-based catalysts. *Catal Today*. (2013);213:87–92.
30. Ermakova MA, Ermakov DY, Plyasova LM, Kuvshinov GC. XRD studies of evolution of catalytic nickel nanoparticles during synthesis of filamentous carbon from methane. *Catal Lett*. (1999);62:93–97.

31. Villacampa JI, Royo C, Romeo E, Montoya JA, Angel PD, Monzón A. Catalytic decomposition of methane over Ni-Al_2O_3 coprecipitated catalysts: reaction and regeneration studies. *Appl Catal A*. (2003); 252:363–383.
32. Takenaka S, Kobayashi S, Ogihara H, Otsuka K. Ni/SiO2 catalyst effective for methane decomposition into hydrogen and carbon nanofibers. *J Catal*. (2003);217:79–87.
33. Sinha K, Menendez J. First- and second-order resonant Raman scattering in graphite. *Phys Rev B*. (1990);41:10845–10847.
34. Alvarez WE, Pompeo F, Herrera JE, Balzano L, Resasco DE. Characterization of single-walled nanotubes (SWNT) produced by CO disproportionation on Co-Mo catalyst. *Chem Mater*. (2002);14:1853–1858.

Manuscript received Jun. 26, 2013, and revision received Nov. 25, 2013.